



Razi University

**Faculty of Science
Department of Physics**

Ph. D Thesis

Title:

Preparation and investigation of polymer nanocomposites by using carbon nanotubes coated with nanoparticles and quantum dot for use in targeted drug delivery and industry

Supervisor: Professor Rostam Moradian

By:

Bandar Astinchap

July 2012

Abstract

Carbon nanotubes have unique properties that make them attractive for various applications such as engineering and medicine and also can be used for preparation of nanocomposites with special properties. However, because of some their limitations (like chemical inertness) to make nanocomposites, carbon nanotubes have to be modified by inorganic (nanoparticles) or/and organic (polymer) materials.

In this thesis, we have focused on modification multiwall carbon nanotubes (MWCNTs) by filling their cavities with magnetic nanoparticles and decorating their sidewall with inorganic nanoparticles and polymers to make new nanocomposites.

As it mentioned in chapter 2, we have decorated MWCNTS by SnS₂ nanoparticles with different sizes, using a simple chemical method. Following this approach, MWCNTS functionalized by using acid (sulfuric and nitric) mixture, then this system coated by tin disulfide (SnS₂) nanoparticles with nanoparticle sizes controlling. The samples have been characterized by X-Ray diffraction (XRD) and transmission electron microscope (TEM). We found size and uniformity of the SnS₂ nanoparticles influenced by increasing of reaction temperature and time. By increasing reaction temperature and time, size of the SnS₂ nanoparticles became larger and less uniform. Also we found ultrasound waves could be used instead of organic compounds for avoiding agglomeration of the SnS₂ nanoparticles on the surface of MWCNTs.

In chapter 3 we have described an improved method to decorate (MWCNTs) by anatase titanium dioxide (TiO₂) nanoparticles via the precipitation of TiCl₄ precursor on the modified acid oxidized MWCNTs by using poly citric acid dendrimer and used in preparation of nanocomposite polyethersulfone (PES) membranes. We have modified MWCNTs by grafting poly citric acid dendrimer to functional groups on the MWCNTs by "grafting from" method. In this way, the functional groups and active sites onto surface of MWCNTs increased and the TiO₂ nanoparticles have been coated on the MWCNTs better and more uniform then without dendrimer grafting. TiO₂ coated MWCNTs were characterized by TEM, XRD and atomic force microscopic (AFM). The analyses showed that the TiO₂ nanoparticles on the surface of MWCNTs had anatase nanostructure with size in the range of 10–20 nm. Then our colleagues at Prof. Madaeni's group in Membrane Research Center (Vahid Vatanpour, Sayed Siavash Madaeni and Sirius Zinadini) the effect of embedding TiO₂ coated MWCNTs in PES matrix on membrane morphology, properties and antibiofouling were investigated and the

obtained results were compared with the prepared oxidized MWCNTs and TiO₂ blended PES membranes.

In chapter 4, we have synthesized novel fluorescence magnetic nanocomposites by multi-functionalized (MWCNTs) which containing super paramagnetic Fe₃O₄ nanoparticles, ZnS quantum dots and liner dendritic copolymer (poly citric acid and polyethylene glycol) (PCA-PEG-PCA). These nanocomposites are prepared by two methods: covalent and noncovalent, so that at first MWCNTs are opened and functionalized by -COOH and -OH groups using a mixture of sulfuric and nitric acids. Then the provided system filled by superparamagnetic nanoparticles (Fe₃O₄ nanoparticles) through wet chemistry method and filled MWCNTs coated by ZnS quantum dots. Finally ZnS/Fe₃O₄@MWCNT-graft-dendrimer nanocomposites are synthesized by two methods: (1) grafting poly citric acid chains to the functional groups on the MWCNTs using melting mixture of poly condensation of monohydrate citric acid and functionalized Fe₃O₄@MWCNT in the vacuum (covalent) and (2) liner dendretic copolymer (PCA-PEG-PCA) is synthesized by polymerization method under vacuum then for preparation nanocomposite, dendrimer attached to ZnS/Fe₃O₄@MWCNT (noncovalent). By comparing hysteresis loops of these bionanocomposites with different methods synthesized, we found their magnetic properties could be controlled and be saved by noncovalent methods. Our results show that the magnetic composites are superparamagnetic, which is a necessary and an important property for magnetic targeting carriers. For show in vitro drug release, we conjugate Paclitaxel (PTX) as anti cancer drug to liner dendritic copolymer (PCA-PEG-PCA) onto modified MWCNTs and investigated drug release at difference conditions of pH, which shows higher release at pH 5. The structure of nanocomposites was characterized and investigated by different methods like TEM, XRD, thermogravimetric analysis (TGA), Vibrating sample magnetometer (VSM) and Fourier transform infrared (FT-IR). These nanocomposites have applications in marking medicines in the cancer therapy with less side effects.

The syntheses of novel nanoarchitectures are an important way to combine several properties into the same nanometric object. Magnetic, catalytic, optical and electrical properties can be embedded and used for heating, moving, or monitoring the nanocomposite. Several nanocomposites are based on carbon nanotubes (CNTs). Owing to the presence of empty cavities and very large surface external area, this allotropic form of carbon is especially suitable for this purpose and particularly for catalytic applications. So for next work where writhed in chapter 5 we decided to try to prepare the nanocomposite based on MWCNTs for catalyst application.

In chapter 5 which is our cooperation with an Italian group at CNR (Rome), we described a new general strategy to synthesize three-block, smart nanocomposites based on MWCNTs by a wet method. The new bifunctional material is shortly referred to as FePt@MWCNTs/Ru(NPs) to point out that nanoparticles (NPs) of a magnetically soft alloy (FePt fcc) fill the MWCNTs cavity, while catalytic Ru NPs decorate the external wall. In this way well separated catalytic and magnetic NPs are obtained. All the synthetic steps are described in detail. TEM, HRTEM, XRD and magnetic measurements by VSM are used to monitor all the steps and to prove the effectiveness of the method.

Table of contents

Abstract	
Dedication	
Acknowledgment	
Table of contents	
List of tables	
List of figures	
CHAPTER 1: Introduction and literature review	
1.1. Background	2
1.2. History of nanotubes	2
1.3. AN OVERVIEW or CARBON NANOTUBES	3
1.3.1. Structure of nanotubes	3
1.3.2. Properties of nanotubes.....	5
1.3.3. Electronic properties.....	5
1.3.4. Transport properties.....	6
1.3.5. Vibrational properties	7
1.3.6. Mechanical properties.....	8
1.3.7. Synthesis of Carbon Nanotubes	11
1.3.8. Functionalization of Carbon Nanotubes	16
1.3.9. Some Applications of Functionalized Carbon Nanotubes	26
1.10. OBJECTIVES.....	26
CHAPTER 2: Synthesis and control size of SnS ₂ nanoparticles on the surfacemulti-walled carbon nanotubes.....	
2. 1. Introduction	29
2. 2. Experimental	30
2. 3. Results and Discussion.....	30
2. 4. Conclusions	33
CHAPTER 3: Decorate MWCNTs with TiO ₂ nanoparticles by poly citric acid dendrimer and use in preparation of nanocomposite polyethersulfone (PES) membranes.....	
3. 1 Introduction.....	36
3. 2 Experimental.....	37
3. 2. 1 Materials.....	37

3. 2. 2. Preparation of modified MWCNTs.....	38
3. 2. 3. Preparation of TiO ₂ coated multiwalled carbon nanotube.....	38
3. 2. 4. Fabrication of asymmetric mixed matrix TiO ₂ coated MWCNTs/PES	
Membranes	40
3.3. Characterization	40
3.4. Results and discussion.....	41
3.4.1. Characterization of oxidized MWCNTs	41
3.4.2. Characterization of TiO ₂ coated multiwalled carbon nanotubes....	42
 CHAPTER 4:	
4.1. Introduction	47
4.2. Experimental	49
4.2.1 Opening MWCNTs	49
4.2.2. Filling of MWCNTs	49
4.2.3. Polymerization of citric acid onto Fe ₃ O ₄ @MWCNT for preparation of Fe ₃ O ₄ @MWCNT-g-PCA nanocomposites	50
4.2.4. Coated filled MWCNTs by ZnS.....	51
4.2.5. Synthesis of PCA-PEG-PCA Copolymers.....	51
4.2.6. Preparation of magnetic nanocarrier	51
4.2.7. Preparation of magnetic/fluorescence nanocarrier-Paclitaxel conjugate (MFNC- PTX).....	52
4.3. Characterization	52
4.4. Results and Discussion.....	52
4.5. Conclusions	67
 CHAPTER 5: Bifunctional FePt@MWCNTs/Ru nanoarchitectures: synthesis and characterization	
5.1. Introduction	67
5.2. Experimental section.....	72
5.3. RESULTS AND DISCUSSION.....	73
5.3.1. Synthesis of nanocomposite.....	73
5.3.1.1 Filling with FePt NPs and washing.....	73
5.3.1.2 Synthesis of the starting salt.....	74
5.3.1.3 Filling procedure.....	74
5.3.1.4 Cleaning the external wall.....	75
5.3.1.5 Reduction of [Fe(H ₂ O) ₆][PtCl ₆].....	77
5.3.2 Decoration with Ru NPs.....	78

5.3.2.1 FePt@MWCNTs acid re-functionalization.....	78
5.3.2.2 The cavities protection.....	79
5.3.2.3 Decoration with Ru NPs	80
5.4. CONCLUSIONS	84

List of tables

Table 2-1	Preparation condition and size of SnS ₂ nanoparticles coated MWCNTs	32
Table 3-1	Viscosity of different polyethersulfone casting solution at 25 °C.....	44

List of figures

Figure 1-1	Schematic diagrams of (a) single-wall nanotube (SWNT) and (b) multi-wall nanotube (MWNT).....	2
Figure 1-2	Schematic diagram showing how a hexagonal sheet of graphite is “rolled” to form a CNT.....	4
Figure 1-3	The Stone-Wales transformation occurring in an armchair nanotube under axial tension.....	5
Figure 1-4	Density of states (DOS) exhibiting the valence-band (negative values) and conduction-band(positive values) and the Fermi energy (E_f ; centered at 0 eV) for (a) a metallic armchair (5,5) tube, which shows electronic states at the E_f (characteristic of a metal) (b) a zigzag tube revealing semiconducting behavior caused by the energy gap located between the valence and conduction band (characteristic of semiconductors). The spikes shown in the DOS of the tubes are called van Hove singularities and are the result of the one-dimensional quantum confinement, which is not present in an infinite graphite crystal	6
Figure 1-5	(a) Phonon dispersion of 2-D graphite using the force constants from Reference (b) the phonon density of states for a 2-D graphene sheet. (c) The calculated phonon dispersion relations of an armchair CNT with $(n, m) = (10, 10)$, for which there are 120 degrees of freedom and 66 distinct phonon branches calculated from (a) by using the zone-folding procedure. (d) The corresponding phonon density of states for a (10,10) nanotube	7
Figure 1-8	(a) AFM image of a SWNT rope adhered to the polished alumina ultrafiltration membrane, with a portion bridging the pore of the membrane. (b) Schematic of the measurement: the AFM is used to apply a load to the nanobeam and to determine directly the resulting deflection	9
Figure 1-9	Morse potential	10
Figure 1-10	Unit cells for (a) (5,5) armchair nanotube and (b) (9,0) zig-zag nanotube	11
Figure 1-11	Theoretical strength of SWNTs as a function of diameter	11

Figure 1-12	Oven laser vaporization apparatus.....	13
Figure 1-13	Schematic of the reactor used for the nanotube synthesis from ferrocene xylene mixture	
Figure 1-14	Schematic drawing of the formation process of CNTs by chemical vapor deposition method in pores of alumina template.....	15
Figure 1-15	Functionalization possibilities for SWNTs: A) defect group functionalization, B) covalent sidewall functionalization, C) noncovalent functionalization with surfactants, D) noncovalent exohedral functionalization with polymers, and E) endohedral functionalization	
Figure 1-16	Illustration to the Laplace equation.....	18
Figure 1-17	The force balance at the triple line.....	19
Figure 1-18	(a) Stone Wales (or 7-5-5-7) defect on the sidewall of a nanotube(b) Typical defects in SWNT.....	22
Figure 1-19	Schematic of one type of chemical sidewall functionalization of SWNTs.....	23
Figure 1-20	Schematic representation of the chemical modification of CNTs through oxidation followed by the esterification or amidization of the carboxyl groups.....	23
Figure 1-21	Scheme of the solvent free functionalization of CNTs with various 4-substituted anilides and isoamyl nitrite or sodium nitrite/acid.....	24
Figure 1-22	Schematic representation of the Bingel modification of fullerenes. The first step (1) is creation of C-nucleophile by deprotonation of halo-ethers or haloketones; the second step (2) is intermediate; and the third step (3) is cyclopropanation of fullerenes.....	24
Figure 1-23	Schematic representation of chemistry of (i) cyclopropanation of SWNT and the following (ii) transesterification reaction with 2-(methylthio) ethanol for (iii) the covalent attachment of gold nanoparticles; and (iv)fluorine markers for AFM and F NMR, respectively.....	25
Figure 2-1	(a) TEM image and (b) XRD pattern of the SnS ₂ /MWCNTs nanocomposites for S1.....	31
Figure 2- 2	XRD patterns of SnS ₂ /MWCNTs nanocomposites at different condition: (a) S2, (b) S3 and (c) S4.....	32
Figure 2-3	TEM image of the different SnS ₂ coated MWCNTs: (a) S2 and (b) S4... ..	33
Figure 3-1	The schematic of preparation of TiO ₂ coated MWCNTs.....	39
Figure 3-2	The FT-IR spectra of raw MWCNTs (a) and oxidized MWCNTs (b).	41
Figure 3-3	TEM image of TiO ₂ coated MWCNT.....	42

Figure 3-4	XRD pattern of (Right) MWCNTs and (Left) TiO ₂ coated MWCNTs	43
Figure 3-5	The schematic mechanism illustration of photocatalytic activity of TiO ₂ coated MWCNTs	43
Figure 4-1	Illustrates covalent synthesis process of Fe ₃ O ₄ @MWCNTs-g-PCA nanocomposite	53
Figure 4-2	Illustrates noncovalent synthesis process of ZnS/Fe ₃ O ₄ @MWCNTs/PCA-PEG-PCA nanocomposite	54
Figure 4-3	Show FT-IR spectra of: (a) Pristine MWCNTs (b) functionalized MWCNT and (c) Fe ₃ O ₄ @MWCNTs-g-PCA nanocomposite (d) ZnS/Fe ₃ O ₄ @MWCNTs/Dendrimer nanocomposites	55
Figure 4-4	Shows TEM image of encapsulated Fe ₃ O ₄ clusters into the MWCNT	56
Figure 4-5	Illustrates TEM images of Fe ₃ O ₄ @MWCNTs-g-PCA nanocomposites with a scale bar of (a) 200 nm and (b) 40 nm	57
Figure 6	Illustrates XRD patterns of magnetic MWCNT nanocomposite.....	58
Figure 4-8	Shows hysteresis loops of (a) Fe ₃ O ₄ @MWCNTs, (b)ZnS/Fe ₃ O ₄ @MWCNTs/dendrimer (c) Fe ₃ O ₄ @MWCNTs-g-PCA nanocomposite	59
Figure 4-9	Illustrates TEM images of (a) ZnS/Fe ₃ O ₄ @MWCNTs nanocomposites and (b) ZnS/Fe ₃ O ₄ @MWCNTs-g-dendrimer.....	60
Figure 4-10	Illustrates XRD patterns of ZnS/Fe ₃ O ₄ @MWCNTs-g-Dendrimer nanocomposites.....	61
Figure 4-11	¹ HNMR spectrum of Linear–dendritic macromolecules grafted to multi functionalized MWCNTs	62
Figure 4-12	The PL spectra of nanocomposites	63
Figure 4-13	Illustrates TGA diagrams of: (a) MWCNTs, (b) PCA-PEG-PCA (c) ZnS/Fe ₃ O ₄ @MWCNTs-g-Dendrimer	64
Figure 4-14	DLS of (a) PCA-PEG-PCA, (b) ZnS/Fe ₃ O ₄ @MWCNTs and (c)ZnS/Fe ₃ O ₄ @MWCNTs/polymer	64
Figure 4-15	Luminescence image of the magnetic nanocomposite	65
Figure 4-16	(a) Shows a photo of synthesized Fe ₃ O ₄ @MWCNTs-g-PCA nanocomposite (left) and MWCNTs (right) in water. (b) noncovalent modification of MWCNTs. (c) effected of external magnetic filed onto magnetic nanocomposite	66
Figure 4-17	Release profiles of PTX from magnetic nanocarrier at different conditions	67
Figure 5-1	Schematic representation of final nanocomposite of the synthesis study	73

Figure 5-2	a) TEM b) HRTEM of MWCNTs. c) and d) TEM e) and f) of FePt filled MWCNTs.....	75
Figure 5-3	Schematic representation of the FePt@MWCNTs nanocomposite synthesis a) nanocomposite with the starting salt inside and outside MWCNTs. b) The washing procedure with benzene protection. c) nanocomposite with starting salt only inside MWCNTs. d) The reduction step. e) FePt inside MWCNTs indicate as FePt@MWCNTs	76
Figure 5-4	XRD patterns of opened (down), filled with FePt (middle), filled with FePt and Ru decorated MWCNTs (top).....	78
Figure 5-5	The synthesis of final nanocomposite starting from FePt(fcc)@MWCNTs protect by mesitylen.....	80
Figure 5-6	a)- d) TEM, HRTEM and SAED of FePt@ MWCNTs/Ru. The images e) and f) are obtained from lower concentration of RuCl ₃ precursor in the synthesis	82
Figure 5-7	Results of the synthesis without protection or with benzene protection; a) Ru decoration, b) Ru NPs inside MWCNTs, c-e) FePt/Ru core-shell NPs inside MWCNTs.....	83
Figure 5-8	Room temperature magnetization curves of open MWCNTs (– ● –), FePt@MWCNTs (– ○ –) and FePt@MWCNTs:Ru (– Δ –) samples. The curves are normalized to the total weight in (a) and to the saturation magnetization in (b, c).....	84

Chapter 1

INTRODUCTION AND LITERATURE REVIEW

CHAPTER 1. LITERATURE REVIEW

In this chapter we will overview the history of the discovery of carbon nanotubes, the methods of their synthesis, and the unique properties of carbon nanotubes, which depend on the synthesis method. Then we will discuss some of the most common methods of functionalization of carbon nanotubes for modified them to make nanocomposites. At the end of the chapter we will show various applications of modified nanotubes.

1. 1. Background

Carbon nanotubes are unique nanostructures with extraordinary electronic and mechanical properties. Interest from the scientific community first focused on their outstanding electronic properties. As other useful properties have been discovered, particularly mechanical properties, interest has grown in potential applications.

An ideal nanotube can be thought of as a hexagonal network of carbon atoms rolled up to make a seamless cylinder. Just a nanometre in diameter, the cylinder can be tens of microns long, and each end is "capped" with half of a fullerene molecule. CNTs exist in two categories (Figure 1-1): (1) single-wall nanotubes which possess the fundamental cylindrical structure, and (2) multi-wall nanotubes which are made of coaxial cylinders, with spacing between the layers close to that of the interlayer distance in graphite (0.34 nm).

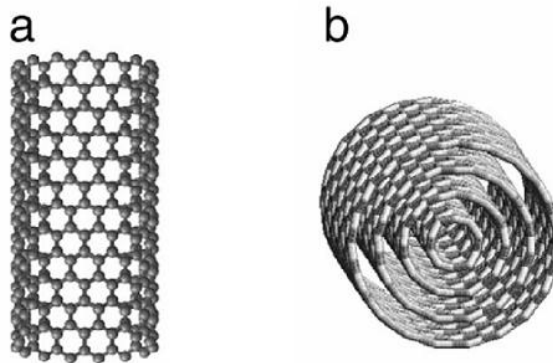


Figure 1-1 Schematic diagrams of (a) single-wall nanotube (SWNT) and (b) multi-wall nanotube (MWNT)[1].

1.2 History of nanotubes

The first CNTs were prepared by M. Endo in 1978, as part of his Ph. D studies at the University of Orleans in France. He produced very small diameter filaments (about 7 nm)

using a vapour-growth technique, but these fibres were not recognized as nanotubes and were not studied systematically.

It was only after the discovery of fullerenes, C_{60} , in 1985 by Kroto *et al.* [2] that researchers started to explore carbon structures further. In 1991, when the Japanese electron microscopist Sumio Iijima [3] observed CNTs, the field really started to advance.

He was studying the material deposited on the cathode during the arc-evaporation synthesis of fullerenes and he came across CNTs.

A short time later, Thomas Ebbesen and Pulickel Ajayan, from Iijima's lab, showed how nanotubes could be produced in bulk quantities by varying the arc-evaporation conditions. But the standard arc-evaporation method had produced only multiwall nanotubes. After some research, it was found that addition of metals such as cobalt to the graphite electrodes resulted in extremely fine singlewall nanotubes. The synthesis in 1993 of SWNTs was a major event in the development of CNTs [4, 5].

Although the discovery of CNTs was an accidental event, it opened the way to a flourishing research into the properties of CNTs in labs all over the world, with many scientists demonstrating promising physical, chemical, structural, electronic, and optical properties of CNTs.

1.3. AN OVERVIEW or CARBON NANOTUBES

There is extensive literature on nanotube structure and its physical and chemical properties. During almost two decades, different methods for nanotube synthesis and functionalization have been developed. Because of recent progress in nanotube syntheses, the focus of research has shifted from synthesis, purification, and characterization of nanotube chemical and physical properties to nanotube functionalization and applications.

1.3.1. Structure of nanotubes

The primary symmetry classification of a CNT divides them into achiral or chiral [6]. An achiral nanotube is defined by a nanotube whose mirror image has an indistinguishable structure to the original one. And, as a consequence, it is superimposable to it. There are only two cases of achiral nanotubes: armchair and zig-zag nanotubes.

The simplest way of specifying the structure of an individual tube is in terms of a vector, the chiral vector (C_h) joining two equivalent points on the original graphene lattice. The cylinder is produced by rolling up the sheet such that the two end-points of the vector are superimposed (Figure 1-2).

The chiral vector can be defined in terms of the lattice translational indices (n, m) and the basic vectors a_1 and a_2 of the hexagonal lattice and corresponds to a section of the nanotube perpendicular to the nanotube axis.

$$C_h = na_1 + ma_2 \quad (m, n \text{ are integers}, 0 \leq |m| \leq n) \quad (1-1)$$

The chiral angle, θ , is defined as the angle between the vectors C_h and a_1 , with values of θ in the range $0^\circ \leq \theta \leq 30^\circ$, due to the hexagonal symmetry of the honeycomb lattice.

$$\cos \frac{C_h \cdot a_1}{|C_h||a_1|} = \frac{2n+m}{2\sqrt{n^2+m^2+nm}} \quad (1-2)$$

The chiral angle θ denotes the tilt angle of the hexagons with respect to the nanotube axis, and the angle θ specifies the spiral symmetry. The two limiting cases, corresponding to the achiral nanotubes, exist where the chiral angle is at 0° (zig-zag) and 30° (armchair).

The diameter of the CNT (d_t) is given by L/π , in which L is the circumferential length of the CNT:

$$d_t = \frac{L}{\pi} \quad (1-3)$$

$$L = |C_h| = \sqrt{C_h \cdot C_h} = a\sqrt{n^2 + m^2 + nm} \quad (1-4)$$

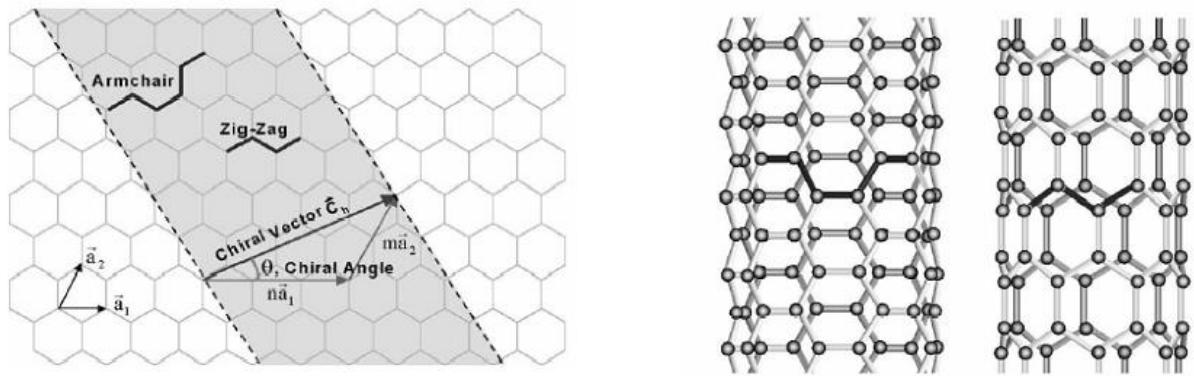


Figure 1-2. Schematic diagram showing how a hexagonal sheet of graphite is “rolled” to form a CNT [7].

Although the chirality has a relatively small influence on the elastic stiffness, the Stone-Wales transformation (Figure 1-3), a reversible diatomic interchange where the resulting structure is two pentagons and two heptagons in pairs, plays a key role in the nanotube plastic deformation under tension.

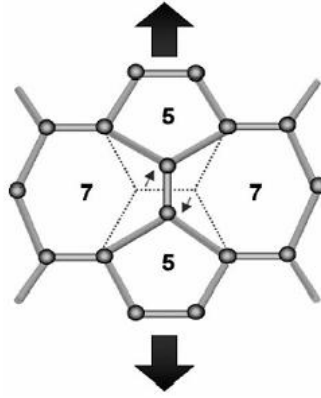


Figure 1-3. The Stone-Wales transformation occurring in an armchair nanotube under axial tension [7].

1.3.2. Properties of nanotubes

1.3.3. Electronic properties

The previously mentioned differences in chirality play an important role in the electronic properties of CNTs. Theoretical studies on the electronic properties of CNTs indicate that all armchair tubes have metallic band-structure, as well as zigzag nanotubes exhibiting values of m, n multiples of three [8, 9]. In summary, the metallic transport condition for nanotubes can be expressed as:

$$\frac{(2m+n)}{3} = \text{integer} \quad (1-5)$$

It is noteworthy that SWNTs can be either metallic or semiconducting depending on the choice of (m,n) , although there is no difference in the chemical bonding between the carbon atoms within the nanotubes and no doping or impurities are present (Figure 1-4).

The unique electronic properties of CNTs are caused by the quantum confinement of electrons normal to the nanotube axis. In the radial direction, electrons are confined by the monolayer thickness of the graphene sheet. Consequently, electrons can propagate only along the nanotube axis, and so to their wave vector points. The resulting number of one-dimensional conduction and valence bands effectively depend on the standing waves that are set up around the circumference of the carbon nanotube. The sharp intensities (spikes) shown in the density of states (DOS) of the tubes are known as van Hove singularities and are the result of this one-dimensional quantum conduction (Figure 1-4) that is not present in an infinite graphite crystal [10].

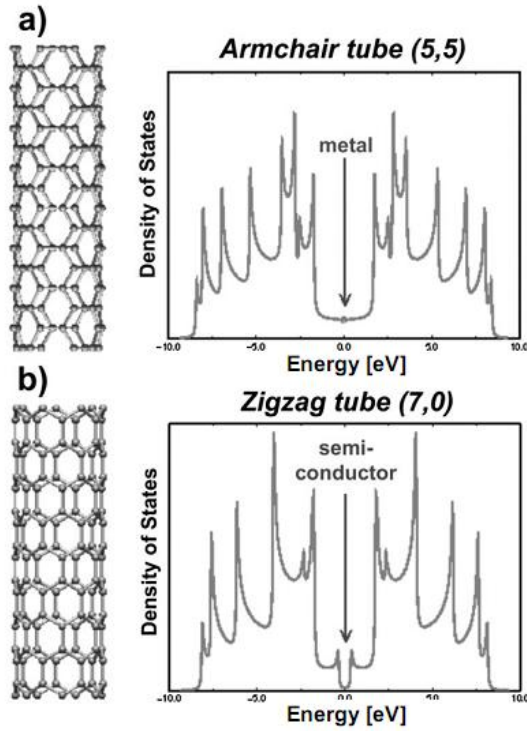


Figure 1-4. Density of states (DOS) exhibiting the valence-band (negative values) and conduction-band (positive values) and the Fermi energy (E_f ; centered at 0 eV) for (a) a metallic armchair (5,5) tube, which shows electronic states at the E_f (characteristic of a metal) (b) a zigzag tube revealing semiconducting behaviour caused by the energy gap located between the valence and conduction band (characteristic of semiconductors).

The spikes shown in the DOS of the tubes are called van Hove singularities and are the result of the one-dimensional quantum confinement, which is not present in an infinite graphite crystal [11].

MWNTs are more complex objects than SWNTs since each one of their carbon shells can have different electronic character and chirality. However, in studies of MWNTs with a metallic outer shell that are side-bonded to metal electrodes, it was concluded that electrical transport at low energies is dominated by outer-shell conduction [12].

1.3.4. Transport properties

Theoretical conductivity

In a macroscopic conductor, the resistivity, ρ , and the conductivity, σ , are physical properties of a material. However, when the size of the conductor becomes small compared to the characteristic lengths for the motion of electrons, then ρ and σ will both depend on the dimension L through quantum effects. The quantized resistance of a CNT (R_0) has been calculated [6] and is equal to

$$R_0 = \frac{h}{2e^2} = 12.9064 \times 10^3 \Omega \quad (1-6)$$

The inverse of R_0 gives the quantized conductance G_0 by

$$G_0 = \frac{1}{R_0} = \frac{2e^2}{h} = 77.4809 \times 10^{-6} S \quad (1-7)$$

Ponchral *et al.* [13] measured the resistivity of nanotubes using a scanning probe microscope (SPM). They obtain a value of $\rho < 100 \Omega/\mu m$.

Chemical doping of SWNTs with electron donors or acceptors has been used to enhance their electrical conductivity in analogy to the well-known graphite intercalation compounds.

1.3.5. Vibrational properties

Phonon structure

Phonons denote the element of motion or quantized normal mode vibrations of a system. The graphene sheet has two atoms per unit cell, thus having six phonon branches (Figure 1-5(a) and 1.5(b)). As for the electronic properties, the phonon dispersion relations and phonon density of states (DOS) for SWNTs can be deduced from those of the graphene sheet [6, 14].

The phonon dispersion for a (10,10) SWNT obtained by a zone-folding procedure is illustrated in Figure 1-5(c), and the respective phonon DOS is shown in Figure 1-5(d).

The large amount of sharp structure in the phonon density of states in Figure 1-5(d) for the (10,10) SWNT reflects the many phonon branches and the one dimensional nature of SWNTs relative to two dimensional graphite arising from the quantum confinement of the phonon states in van Hove singularities [6, 14].

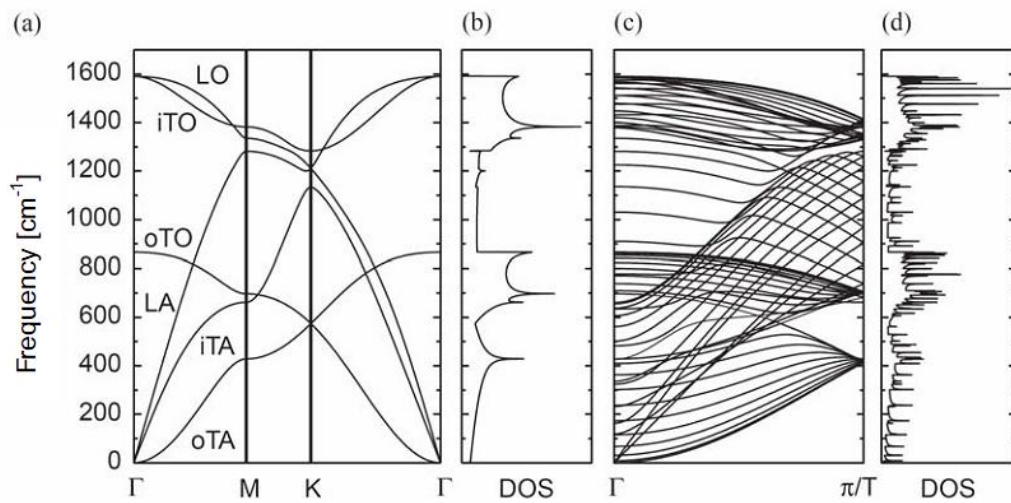


Figure 1-5. (a) Phonon dispersion of 2-D graphite using the force constants from Reference [15]. (b) The phonon density of states for a 2-D graphene sheet. (c) The calculated phonon dispersion relations of an armchair CNT with $(n, m) = (10, 10)$, for which there are 120 degrees of freedom and 66 distinct phonon branches [6],

calculated from (a) by using the zone-folding procedure. (d) The corresponding phonon density of states for a $(10,10)$ nanotube [14].

1.3.6. Mechanical properties

In this paragraph, a review of the most important results for the measurement of the mechanical properties of CNTs will be presented. Then, these results will be critically discussed and compared with commercial fibres. However, in order to have a more accurate idea of the real potential of CNTs as reinforcing fillers for composite materials, a clear definition of the cross-sectional area of the nanotube needs to be introduced. In fact, the majority of the studies presented in literature assumed that only the external layer of nanotubes carried the load. Hence they used only the area occupied by the external wall as cross-sectional area, ignoring the hollow part of the nanotube. However, this assumption leads to an overestimate of the nanotube's mechanical properties. When nanotubes are used as reinforcing fillers in nanocomposites, the whole volume they occupy needs to be considered in micromechanical models, hence their whole cross-sectional area including the hollow part should be considered. For this reason, the nanotubes effective properties will be calculated.

Young's modulus

The Young's modulus, E , of a material is directly related to the cohesion of the solid and therefore to the chemical bonding of the constituent atoms. Since the sp^2 carbon-carbon bond is one of the strongest of all chemicals bonds, a structure based on a perfect arrangement of these bonds oriented along the axis of a fibre would produce an extremely strong material. When CNTs were discovered, their structure immediately encouraged speculation about their potential mechanical properties.

In 1996 Treacy and co-workers measured indirectly the Young's modulus of multiwall nanotubes made by arc-discharge [16]. They used a transmission electron microscope (TEM) to measure the amplitude of their intrinsic thermal vibrations and they calculated the Young's modulus for a number of nanotubes. Their values ranged from 0.42 to 4.15 TPa. They suggested a trend for higher moduli with smaller tube diameters.

The first direct measurement was performed by Wong et al. in 1997 [17]. They measured the stiffness constant of arc-grown MWNTs clamped at one end using atomic force microscopy (AFM). They obtained an average of 1.28 ± 0.59 TPa with no dependence on tube diameter. Two years later, Salvetat *et al.* [18] used a similar method. They clamped the

MWNTs at both ends over a pore in a polished alumina ultrafiltration membrane and measured an average of 810 ± 410 GPa. Measurements on SWNTs soon followed and Salvétat et al. used their AFM method to measure an average modulus of 1 TPa [19] (Figure 1-8).

Lourie and Wagner used micro-Raman spectroscopy to measure the compressive deformation of a nanotube embedded in an epoxy matrix. For SWNT, they obtained an extremely high value for the Young's modulus of 2.8-3.6 TPa, while for MWNT they measured 1.7-2.4 TPa [20].

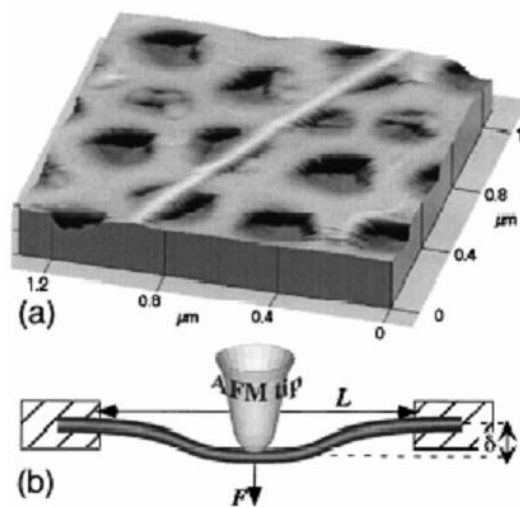


Figure 1-8. (a) AFM image of a SWNT rope adhered to the polished alumina ultrafiltration membrane, with a portion bridging the pore of the membrane. (b) Schematic of the measurement: the AFM is used to apply a load to the nanobeam and to determine directly the resulting deflection [19].

Theoretical tensile strength

The calculation of theoretical strength of materials with covalent bonds from the force between two atoms as described by the Morse potential (Figure 1-9) is well known [21]

and was first applied by de Boer in 1936 [22]. The same approach has been later applied to estimate the potential of polymers molecules for high strength fibres, and it could be applied to the calculation of nanotube strength [23].